Reproductive Toxicology 129 (2024) 108671

Contents lists available at ScienceDirect

Reproductive Toxicology

journal homepage: www.elsevier.com/locate/reprotox

Nrf2 deficiency exacerbated pulmonary pyroptosis in maternal hypoxia-induced intrauterine growth restriction offspring mice

Dan Chen [a,1], Ling-yun Man [a,1], Ying-ying Wang [a,1], Wei-ying Zhu [b], Hui-min Zhao [a], Sheng-peng Li [a], Yan-li Zhang [a], Shuai-chao Li [a], Ya-xian Wu [a], Ling-Ai [b,*], Qing-feng Pang [a,**]

[a] Department of physiopathology, Wuxi School of Medicine, Jiangnan University, Wuxi, Jiangsu Province 214122, China
[b] Department of obstetric, Maternity and Child Health Care Affiliated Hospital, Jiaxing University, Jiaxing 314000, China

ARTICLE INFO

Keywords:
Nuclear factor erythroid 2-related factor 2
Pyroptosis
Lung development
Hypoxia
intrauterine growth restriction

ABSTRACT

Maternal prenatal hypoxia is an important contributor to intrauterine growth restriction (IUGR), which impedes fetal lung maturation and leads to the development of chronic lung diseases. Although evidence suggests the involvement of pyroptosis in IUGR, the molecular mechanism of pyroptosis is still unclear. Nuclear factor erythroid 2-related factor 2 (Nrf2) has been found to potentially interact with gasdermin D (GSDMD), the key protein responsible for pyroptosis, indicating its crucial role in inhibiting pyroptosis. Therefore, we hypothesized that Nrf2 deficiency is a key molecular responsible for lung pyroptosis in maternal hypoxia-induced IUGR offspring mice. Pregnant WT and $Nrf2^{-/-}$ mice were exposed to hypoxia (10.5 % O_2) to mimic IUGR model. We assessed body weight, lung histopathology, pulmonary angiogenesis, oxidative stress levels, as well as mRNA and protein expressions related to inflammation in the 2-week-old offspring. Additionally, we conducted a dual-luciferase reporter assay to confirm the targeting relationship between Nrf2 and GSDMD. Our findings revealed that offspring with maternal hypoxia-induced IUGR exhibited reduced birth weight, catch-up growth delay, and pulmonary dysplasia. Furthermore, we observed impaired nuclear translocation of Nrf2 and increased GSDMD-mediated pyroptosis in these offspring with IUGR. Moreover, the dual-luciferase reporter assay demonstrated that Nrf2 could directly inhibit GSDMD transcription; deficiency of Nrf2 exacerbated pyroptosis and pulmonary dysplasia in offspring with maternal hypoxia-induced IUGR. Collectively, our findings suggest that Nrf2 deficiency induces GSDMD-mediated pyroptosis and pulmonary dysplasia in offspring with maternal hypoxia-induced IUGR; thus highlighting the potential therapeutic approach of targeting Nrf2 for treating prenatal hypoxia-induced pulmonary dysplasia in offspring.

1. Introduction

Adequate oxygen supply is crucial for fetal growth and facilitats lung development throughout pregnancy. Maternal hypoxia before birth has been shown to lead to neonatal pulmonary artery dysfunction and intrauterine growth restriction (IUGR)[1], which is typically characterized by a reduced fetal birthweight below the 10th percentile for gestational age and sex[2], and it independently increases the risk of chronic lung disease in offspring, including bronchopulmonary dysplasia (BPD)[3,4]. Inadequate oxygen exposure result in pulmonary structural alterations involving the parenchyma, airway, and vasculature as an adaptive response, leading to lung functional changes [5]. Individuals aged 8–15

Abbreviations: Caspase, cysteinyl aspartate specific proteinase; Gclm, Glutamate-Cysteine Ligase Modifier Subunit; GSDMD, Gasdermin D; GPX4, Glutathione peroxidase 4; IUGR, Intrauterine growth restriction; LDH, Lactate dehydrogenase; Nrf2, Nuclear factor erythroid-derived 2-like 2; NLRP3, NLR Family Pyrin Domain Containing 3; MMP, Mitochondrial membrane potential; ROS, Reactive oxygen species; SOD, Superoxide dismutase; Txn, Thioredoxin; TNF-α, Tumor necrosis factor alpha.

* Correspondence to: Department of obstetric, Maternity and Child Health Care Affiliated Hospital, Jiaxing University, NO.2468 East Central Road, South Lake district, Jiaxing, Zhejiang, China.

** Correspondence to: Department of physiopathology, Wuxi School of Medicine, Jiangnan University, 1800 Lihu Avenue, Binhu District, Wuxi, Jiangsu Province, China.

E-mail addresses: 13736836830@163.com (Ling-Ai), qfpang@jiangnan.edu.cn (Q.-f. Pang).

[1] Dan Chen, Ling-yun Man and Ying-ying Wang contributed equally to this study.

https://doi.org/10.1016/j.reprotox.2024.108671
Received 20 May 2024; Received in revised form 17 July 2024; Accepted 19 July 2024
Available online 20 July 2024

years who were born preterm with a diagnosis of IUGR exhibited lower forced expiratory volume in 1 second (FEV1) Z-scores[6]. Adult individuals with a history of IUGR displayed impaired alveolar development characterized by reduced alveolar number, increased lung mesenchymal thickness, and decreased surfactant maturation[7,8]. Rats with IUGR experienced significant pulmonary arterial hypertension and remodeling of the pulmonary vasculature[9]. These pulmonary structural abnormalities can persist into adulthood or even worsen over time, leading to compromised lung function[10]. Therefore, it is very important to study the key molecular mechanisms of IUGR induced by maternal hypoxia during pregnancy and to obtain effective treatment methods.

Despite extensive research on the mechanisms of hypoxia-induced IUGR, the precise molecular mechanism underlying this disease remains elusive. Pyroptosis, a recently discovered form of inflammatory programmed cell death[11], involves the activation of gasdermin D (GSDMD), a key protein responsible for pyroptosis. Upon activation, GSDMD undergoes N-terminal cleavage and translocates to the membrane, resulting in the release of inflammatory mediators and ultimately leading to pyroptosis[12]. Exposure to various detrimental factors during pregnancy such as smoking[13], PM2.5 pollution[14], intermittent hypoxia[15], nicotine [16], and sevoflurane anesthesia [17] can induce pyroptosis in different organs of neonatal mice offspring. Specifically, gestational exposure to perfluorooctane sulfonate leads to pulmonary dysplasia in offspring through caspase-3/GSDME-dependent pyroptosis [18,19]. GSDMD-mediated pyroptosis is crucial for the progression of respiratory diseases, particularly sepsis-related acute lung injury[20, 21]. In addition, maternal serum concentrations of GSDMD were found to be higher in IUGR pregnant women[22]. Therefore, although research on the role of pyroptosis in neonatal lung development is still at an early stage, it is gradually being recognized that pyroptosis plays a pivotal role in hypoxia-induced IUGR. However, the specific molecular mechanism underlying IUGR-induced pyroptosis and GSDMD activation remains unclear.

Excessive reactive oxygen species (ROS) is detrimental and it has been revealed that ROS is pivotal for the occurrence of pyroptosis [23, 24]. The nuclear factor (erythroid-derived 2)-like 2 (Nrf2) is a transcription factor and plays key roles in antioxidation[25]. Dysfunction of Nrf2 contributes to the pathogenesis of respiratory diseases such as BPD, acute respiratory distress syndrome, and chronic obstructive pulmonary disease[26]. Various Nrf2 activators like curcumin, sulforaphane, and resveratrol have been identified for their protective effects against different respiratory diseases[27]. Moreover, pregnant mice lacking Nrf2 have been observed to be more susceptible to generating IUGR offspring[28], and it has been found that curcumin attenuates IUGR by activating the Nrf2-mediated antioxidative signaling pathway[29,30]. Additionally, activating Nrf2 by tert-butylhydroquinone effectively inhibits pulmonary pyroptosis in hyperoxia-induced mice with bronchopulmonary dysplasia[31]. Based on these findings, we hypothesized that deficiency of Nrf2 is a key molecular mechanism responsible for pulmonary pyroptosis in maternal hypoxia-induced IUGR offspring mice. Therefore, this study aims to investigate the roles and mechanisms of Nrf2 in lung development among offspring affected by maternal hypoxia-induced IUGR.

2. Materials and methods

2.1. Animal model of maternal hypoxia-induced IUGR

Animal models of maternal hypoxia-induced IUGR were established using Nrf2 knockout and wild-type (WT) mice with a C57BL/6 J background, obtained from the Model Animal Research Center, Nanjing (project No. XM002783). To examine whether pyroptosis and pulmonary dysplasia exist in maternal hypoxia-induced IUGR offspring mice, pregnant C57BL/6 mice were randomly assigned to Control group (n=4) and IUGR group (n=4). To determine whether Nrf2 play role in maternal hypoxia-induced pyroptosis and pulmonary dysplasia in offspring mice, pregnant C57BL/6 mice and Nrf2 knockout (KO) mice were randomly divided into four groups: WT+Control (n=4), $Nrf2^{-/-}$+Control (n=8), WT+IUGR (n=3) and $Nrf2^{-/-}$+IUGR (n=6). Each group of pregnant mice were housed together in the one cage. The IUGR model was established under hypoxia (10.5 % O_2) exposure from gestational day 11.5 to GD17.5, corresponding to the pseudoglandular–canalicular stage of mouse lung development, and then pregnant mice were returned to a normal environment (21 % O_2) until birth[32,33]. The control group consisted of pregnant mice housed under normoxic conditions (21 % O_2) throughout pregnancy. Offspring mice were weighed weekly from birth until 4 weeks old. Both male and female offspring were included in the study. The experiments including histological and molecular biological analyses were performed on offspring at 2 weeks old. At the end of the experiments, each mouse was euthanized by an overdose of pentobarbital sodium (50 mg/kg, intraperitoneally), and the lung tissues were collected. All experiments were conducted in accordance with established guidelines and approved by the Animal Care and Use Committee of Jiangnan University (JN.No20201130c0420720[325]).

2.2. Histological and immunohistochemistry analysis

The mice were dissected to obtain lung tissue samples at PN14. The left lung tissue samples were initially fixed with a 4 % paraformaldehyde solution, followed by immersion in the same solution for 48 hours and subsequent paraffin embedding. The tissues were then sectioned into 4 μm slices, and the lung morphology was observed through hematoxylin and eosin (H&E) staining. Mean linear intercept (MLI) quantification was calculated as previously described[34]. To assess pulmonary vascular development, lung sections were immunostained with a primary antibody against CD31 (Santa Cruz Biotechnology, diluted at 1:100, #sc-46694), followed using a biotinylated secondary antibody and detection of the avidin-biotin complex signal using a 3,3′-diaminobenzidine solution.

2.3. Immunofluorescence staining

The left lung tissue samples were collected and fixed in 4 % paraformaldehyde at 4 ℃ for 12 h and cryo-protected in 20–30 % sucrose. Cryostat sections were prepared for immunofluorescence staining. The Section (4 μm) were blocked with 0.3 % BSA and 0.1 % Triton X-100 in PBS for 40 min at room temperature, and then incubated with mouse anti-GSDMD antibody (Santa Cruz Biotechnology, 1:50, #sc-393581) at 4℃ overnight. After washing with 0.1 % Triton PBS, the sections were incubated with secondary antibody labeled with Alexa Fluor 488 (1:100, Yeasen, #33206ES60) at room temperature for 30 min. Nuclei were counterstained with DAPI (CWBIO, Taizhou, China; #CW20695) for 5 minutes. The immunostaining was visualized using a Zeiss fluorescence microscope (Oberkochen, Germany).

2.4. The content of lactate dehydrogenase (LDH)

The content of LDH in serum was measured by a commercial assay kit (#A020–2, Nanjing Jiancheng Bio Co., Ltd., China) according to the manufacturer's instructions. Briefly, a total of 20 μL of samples were obtained, transferred into a 96-well microplate together with 25 μL matrix buffer and incubated for 15 min at 37℃. Subsequently, 25 μL of formazan dye was added and incubated for another 15 min at 37℃. Finally, the absorbance was read using a standard ELISA plate reader at 450 nm.

2.5. Enzyme-linked immunosorbent assay (ELISA)

The contents of IL-1β (#MM-0040M1), IL-6 (#MM-0163M1), and TNF-α (#MM-0132M1) in lung tissues were measured by ELISA kits (Meimian, Jiangsu, China) in the light of the manufacturer's guidance.

Briefly, lung tissues were homogenized, centrifugated and then added to microplate coated with monoclonal antibody. Meanwhile, the horseradish peroxidase (HRP)-conjugate reagent was also added and incubated together for 60 min at 37℃. Following this, the plate was washed, and developer solution was added. Finally, the absorbance value was detected at 450 nm wavelength by a microplate reader (Bio-Rad, USA).

2.6. Dual-luciferase reporter assay

The GSDMD luciferase reporter plasmid (pGL4.10-GSDMD Promote), containing a segment of the human GSDMD promoter (NM_001166237.1), was purchased from OBiO Technology Corp, Ltd. (Shanghai, China). The luciferase reporter plasmid was co-transfected with pcDNA3.1-Nrf2 plasmids into 293 T cells. After 24 hours of transfection, the lysed 293 T cells were assayed using the Dual-Luciferase Reporter Assay Kit (Vazyme Biotech, China), and the luciferase reporter signals were measured utilizing a plate luminometer (Synergy H4, BioTek Instruments, Inc., Winooski, VT, USA).

2.7. Western blotting

Lung tissues were homogenized in lysis buffer, and the total protein concentration in samples was measured using the BCA reagent kit (Yeasen, Shanghai, China). The proteins (30 μg) were separated by sodium dodecyl sulfate-polyacrylamide gel electrophoresis and transferred onto nitrocellulose membranes in Tris-glycine-methanol buffer. The bands were visualized using enhanced chemiluminescence. GAPDH was used as a loading control to normalize the data. The antibodies used in Western blot are listed in Table 1.

2.8. Real-Time Quantitative Polymerase Chain Reaction (RT-qPCR)

Total RNA from the lung tissue was extracted using Trizol Reagent (Vazyme Biotech, Nanjing, China; R401). Reverse transcription was performed using ReverTraAce qPCR RT kit (Toyobo, Osaka, Japan) and RT-qPCR was then carried out using SYBR Green qRT-PCR Master Mix Kit (Toyobo, Osaka, Japan) on a StepOne Plus system (Thermo Fisher Scientific, Waltham, MA, USA). The primer sequences for mice were listed in Table 2. Quantification was performed employing the $2^{-\Delta\Delta Ct}$ method, with GAPDH serving as the reference gene.

2.9. RNA-sequence data acquirement

The transcriptomic data of GSE12216 was downloaded from the GEO database (https://www.ncbi.nlm.nih.gov/geo/query/acc.cgi?acc=GSE12216) with the platform GPL2986 ABI Human Genome Survey Microarray Version 2. The "limma" package was used to identify the different GSDMD mRNA expression levels between 8 normal placental samples and 8 IUGR placental samples.

2.10. Protein-protein interactions (PPI) networks analysis

The STRING database was used to construct a PPI network of different expressed hub genes as previously reported[35]. And the Cytoscape (3.7.1) was used to perform further analysis, identify, and visualize the PPI networks.

Table 1
List of primary antibodies used in Western blots.

Antibody	Dilution
GSDMD (Abcam, ab209845)	1:1000
GSDMD (Cell Signalling Technology, #96458)	1:1000
Nrf2 (Proteintech group, 16396–1-AP)	1:1000
ATP1A1 (Proteintech group, 14418–1-AP)	1:1000
LambinB (Bioss, bs−1840R)	1:1000
NLRP3 (Cell Signalling Technology, 15101 S) Caspase−1 (ABclonal, A0964) β-actin (Santa Cruz, sc−47778)	1:1000 1:1000 1:1000

Table 2
Primers for Real-Time Quantitative PCR Analysis.

Gene	Primer	Sequence
IL−1β	Forward	5'-CAAGGAGAACCAAGCAACGA−3'
	Reverse	5'-TTTCATTACACAGGACAGGTATAGA−3'
Nrf2	Forward	5′-AAAATCATTAACCTCCCTGTTGAT−3′
	Reverse	5′-CGGCGACTTTATTCTTACCTCTC−3′
SOD1	Forward	5'-AACCAGTTGTGTTGTCAGGAC−3'
	Reverse	5'-CCACCATGTTTCTTAGAGTGAGG−3'
SOD2	Forward	5'-CAGACCTGCCTTACGACTATGG−3'
	Reverse	5'-CTCGGTGGCGTTGAGATTGTT−3'
Gclm	Forward	5'-AGGAGCTTCGGGACTGTATCC−3'
	Reverse	5'-GGGACATGGTGCATTCCAAAA−3'
Txn	Forward	5'-CATGCCGACCTTCCAGTTTTA−3'
	Reverse	5'-TTTCCTTGTTAGCACCGGAGA−3'
IL−6	Forward	5'-ACTTCCATCCAGTTGCCTTCTTGG−3'
	Reverse	5'-TTAAGCCTCCGATTGTGAAGTG−3'
TNFα	Forward	5'-AGGTTCTCTTCAAGGGACAA−3'
	Reverse	5'-GACTTTCTCCTGGTATGAGATAG−3'
IL−18	Forward	5'-GACAGCCTGTGTTCGAGGATATG−3'
	Reverse	5'-TGTTCTTACAGGAGAGGGTAGAC−3'
NLRP3	Forward	5'-TCACAACTCGCCCAAGGAGGAA−3'
	Reverse	5'-AAGAGACCACGGCAGAAGCTAG−3'
Caspase−1	Forward	5'-GGCACATTTCCAGGACTGACTG−3'
	Reverse	5'-GCAAGACGTGTACGAGTGGTTG−3'
GAPDH	Forward	5'-TGTGATGGGTGTGAACCACGAGAA−3'
	Reverse	5'-GAGCCCTTCCACAATGCCAAAGTT−3'

2.11. Statistical analysis

Measurement data were expressed as means ± standard deviation (SD). Comparisons between two groups were performed using Student's unpaired two-tailed t-test. Comparisons among groups were carried out by analysis of variance (ANOVA) with GraphPad Prism followed by Tukey's multiple comparisons test. The Pearson correlation coefficient was used to assess the correlation between the inflammatory cytokines and birth weight. $P < 0.05$ was considered statistically significant.

3. Results

3.1. Antenatal maternal hypoxia resulted in pulmonary dysplasia in offspring mice

To establish an IUGR model, time-mated pregnant mice were exposed to 10.5 % O_2 from GD11.5 to GD17.5 and then returned to a normoxic environment until birth. Maternal hypoxia during pregnancy significantly reduced fetal birth weight (P=0.0144) (Fig. 1A). The lower body weight sustained on PN7 (P=0.0287), then IUGR offspring exhibited weight gain and displayed catch-up growth with no significant difference in body weight between the Normal and IUGR offspring on PN14 (P=0.3514), 21 (P=0.4431) and 28 days (P=0.1793) (Fig. 1B). To investigate lung development in IUGR offspring, H&E staining was performed (Fig. 1C) which revealed alveolar simplification and collapse with thickening of the alveolar walls as evidenced by a significantly decreased MLI in IUGR offspring (P=0.0200) (Fig. 1D). Additionally, immunohistochemistry staining for CD31, an endothelial cell marker, was conducted (Fig. 1E) which showed no significant difference in CD31 immunoreactivity between the Control and IUGR groups (Fig. 1F). Moreover, considering their involvement in mediating vascular sprouting, proliferation, and endothelial cell migration as well as promoting angiogenesis[36], mRNA levels of VEGFA and VEGFR2 were determined. Both mRNA levels of VEGFA (P=0.0153) (Fig. 1G) and VEGFR2 (P=0.0048) (Fig. 1H) were reduced in the lungs of IUGR offspring. These results indicate that maternal hypoxia during pregnancy triggers pulmonary dysplasia in mice offspring.

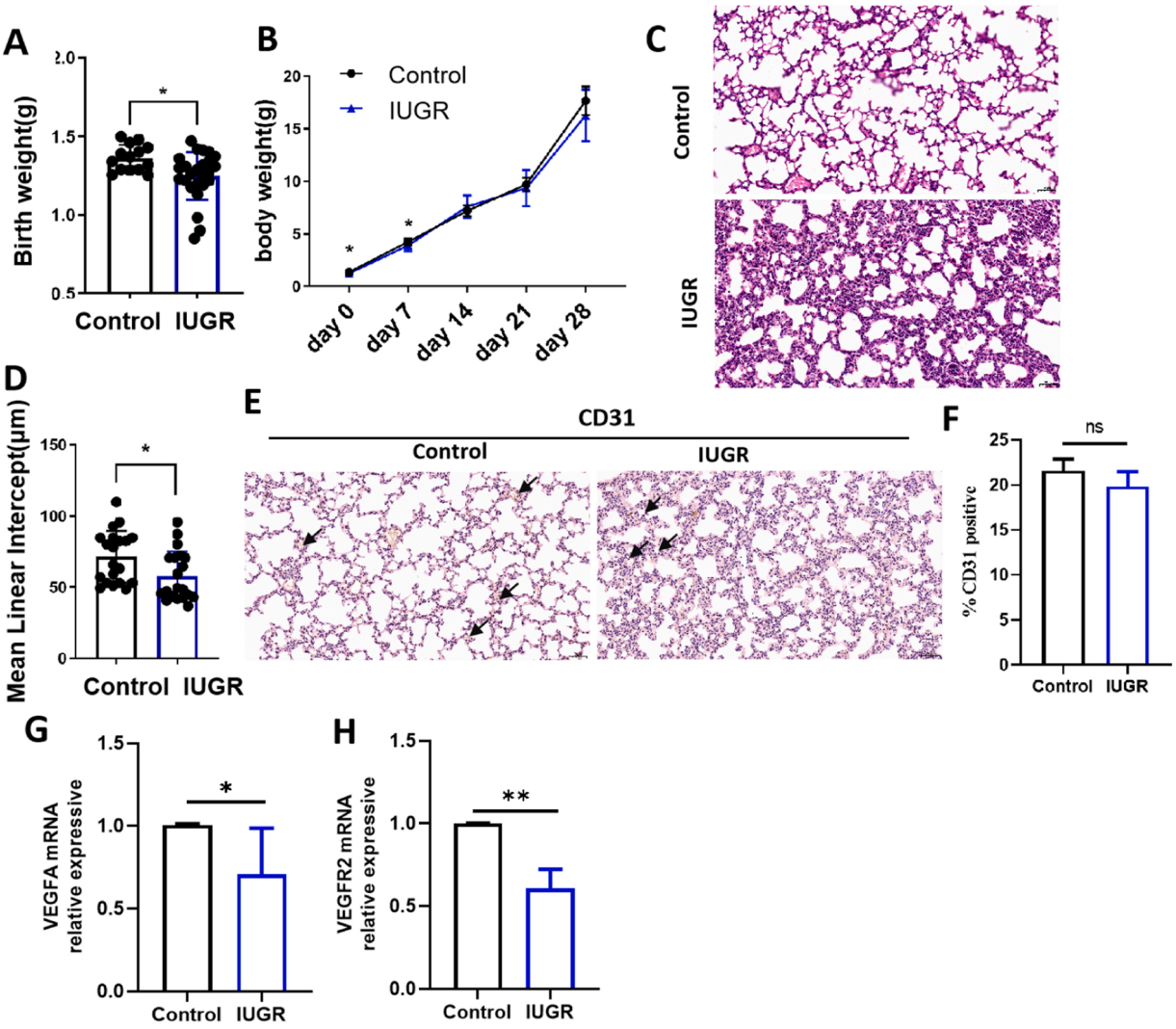

Fig. 1. Chronic maternal hypoxia resulted in IUGR and pulmonary dysplasia in the offspring. (A) Birthweight (control group, n=14; IUGR group, n=25). (B) Mean postnatal weight of offspring (control group, n=14; IUGR group, n=25). (C) Representative H&E stained lung sections (magnification, ×200). (D) Quantification of mean linear intercept (MLI) (n=20). (E) Immunohistochemistry for CD31 in the lung section (magnification, ×200). (F) %CD31 positive cells (n=20). (G-H) Relative mRNA levels of VEGFA and VEGFR2 (control group, n=4; IUGR group, n=5). The data represent the mean±SD. Unpaired 2-sided t-test. Individual *P*-values are denoted above the comparison lines (*$P < 0.05$ vs control).

3.2. Maternal hypoxia during pregnancy induced the expression of pyroptosis-related genes in the lungs of IUGR offspring mice

We have previously observed a significant upregulation of GSDMD (the key protein responsible for pyroptosis) expression in IUGR placenta samples through the GEO database (n=8, *P*=0.0241) (Fig. 2A). To explore whether pyroptosis exists in lung tissues of IUGR offspring, protein content of pyroptosis-related genes in lung tissue were examined as shown in Fig. 2B. It revealed an increase in NLRP3 (*P*=0.0366) (Fig. 2C), Caspase-1 p17 (*P*=0.0139) (Fig. 2D), and GSDMD-N (an executor of pyroptosis) on cell membranes (*P*=0.0095) (Fig. 2E), indicating the presence of pyroptosis in lungs of IUGR offspring. Moreover, serum LDH content was increased in IUGR mice, which also indicating increased pyroptosis (*P*=0.0284) (Fig. 2F). Furthermore, mRNA levels of downstream cytokines associated with pyroptosis, such as IL-6, IL-1β and TNF-α were also examined. Maternal hypoxia during pregnancy significantly elevated IL-6 (*P*=0.0029) and IL-1β (*P*=0.0256) mRNA levels in IUGR mice (Fig. 2G). Moreover, these levels exhibited a negative correlation with birth weight: IL-6 showed a correlation coefficient of r=-0.5769 with P=0.0044 (Fig. 2H), while IL-1β had a correlation coefficient of r=-0.5637 with P=0.0039 (Fig. 2I). However, no significant association was found between TNF-α and birth weight (Fig. 2J). These results provide evidence for the presence of pyroptosis in lungs from maternal hypoxia-induced IUGR offspring.

3.3. The translocation of Nrf2 into the nucleus was hindered in lung tissue of IUGR offspring mice

To investigate the role of Nrf2 in IUGR, we examined the protein levels of Nrf2 and its downstream antioxidant genes. Interestingly, an upregulation of total Nrf2 content was observed in lung tissues of IUGR offspring (*P*=0.0192) (Fig. 3A and B). Subsequently, we assessed the subcellular localization of Nrf2 and found a decrease in nuclear content within lung tissues of IUGR offspring, indicating impaired nuclear translocation (Fig. 3C and 3D). In addition, the Nrf2 downstream antioxidant genes were also examined. The *SOD2* mRNA level was significantly reduced (*P*=0.0153), while there were no significant different on mRNA levels for *SOD1* (*P*=0.12), *Gclm* (*P*=0.152), and *Txn* (*P*=0.087) between control and IUGR group (Fig. 3E). These findings suggest the presence of transcriptional dysfunction involving Nrf2 in lung tissue of IUGR offspring mice resulting in compromised antioxidant defense mechanisms and oxidative damage.

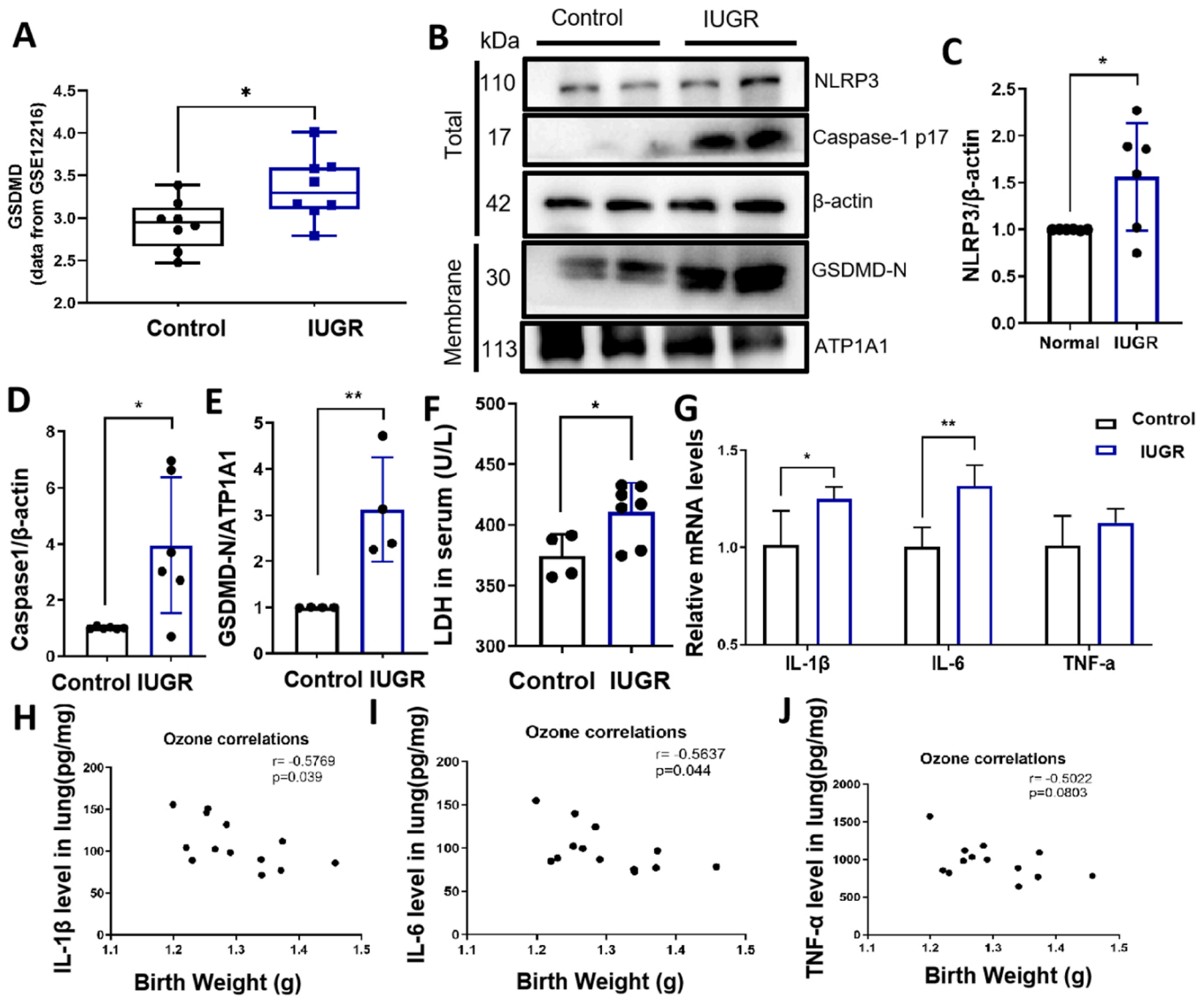

Fig. 2. Maternal hypoxia during pregnancy induced the expressions of pyroptosis-related genes IUGR offspring lungs. (A) Differential gene analysis based on GSE12216 transcriptome data. (B-E) NLRP3, Caspase-1 p17 and GSDMD-N were measured by western blotting. ATP1A1 was used as a membrane loading control and β-actin was used as a total protein loading control. (F) LDH content in serum (control group, n=4; IUGR group, n=7). (G) mRNA expressions of inflammatory cytokines (TNF-α, IL-1β and IL-6) (control group, n=4; IUGR group, n=5). (H-J) Pearson's correlation coefficient analysis of birth weight with cytokines (TNF-α, IL-1β and IL-6) in mouse lung tissue on the day of birth. The data represent the mean±SD. Unpaired 2-sided t-test. Individual P-values are denoted above the comparison lines (*P < 0.05 vs control, **P < 0.01 vs control).

3.4. Nrf2 deficiency resulted in an upregulation of pyroptosis-related gene expression in the lungs of maternal hypoxia-induced IUGR offspring mice

Using the String database (protein-protein interaction), we constructed a network consisting of NLRP3, Caspase1, GSDMD, IL-18, and IL-1β that exhibited significant interactions with Nrf2. The networking graphic in Fig. 4A demonstrated the association between pyroptosis-related genes NLRP3, Caspase1, GSDMD, IL-18 and IL-1β with Nrf2. Through a dual luciferase reporter assay in 293 cells (Fig. 4B), it was revealed that overexpression of Nrf2 inhibited GSDMD transcription. Furthermore, increasing levels of Nrf2 overexpression dose-dependently inhibited not only the expression of GSDMD itself but also its cleavage products GSDMD-N in 293 cells (Supplementary Figure 1). Additionally, to confirm the effect of Nrf2 on pyroptosis, we utilized Nrf2 knockout mice. Our findings indicated that knockout of Nrf2 significantly increased mRNA levels of GSDMD ($P < 0.001$, WT IUGR VS $Nrf2^{-/-}$ IUGR) (Fig. 4C), Caspase-1 ($P < 0.001$, WT IUGR VS $Nrf2^{-/-}$ IUGR) (Fig. 4D), and IL-18 ($P < 0.001$, WT IUGR VS $Nrf2^{-/-}$ IUGR) (Fig. 4E) in lung tissues from IUGR offspring. However, it had no significant effect on the mRNA level of NLRP3 (Fig. 4F). Western blot results demonstrated an up-regulation in GSDMD expression when comparing deficiency of Nrf2 to WT IUGR group samples ($P=0.0165$, WT IUGR VS $Nrf2^{-/-}$ IUGR) (Fig. 4G). Moreover, immunofluorescence staining for GSDMD showed consistent results as well (Figs. 4H and 4I). These results indicate that while inhibiting GSDMD transcription is a function attributed to Nrf2 activity; deficiency or absence thereof leads to an up-regulation in GSDMD expression exacerbating pyroptosis in maternal hypoxia-induced IUGR offspring.

3.5. Nrf2 deficiency aggravated pulmonary dysplasia in maternal hypoxia-induced IUGR offspring

To explore whether Nrf2 play roles in pulmonary pyroptosis of IUGR offspring, Nrf2 knockout mice were used. The IUGR process was significantly exacerbated by the lack of Nrf2, as evidenced by a lower rate of live fetus ($P=0.0436$, WT IUGR VS $Nrf2^{-/-}$ IUGR) and birth weight

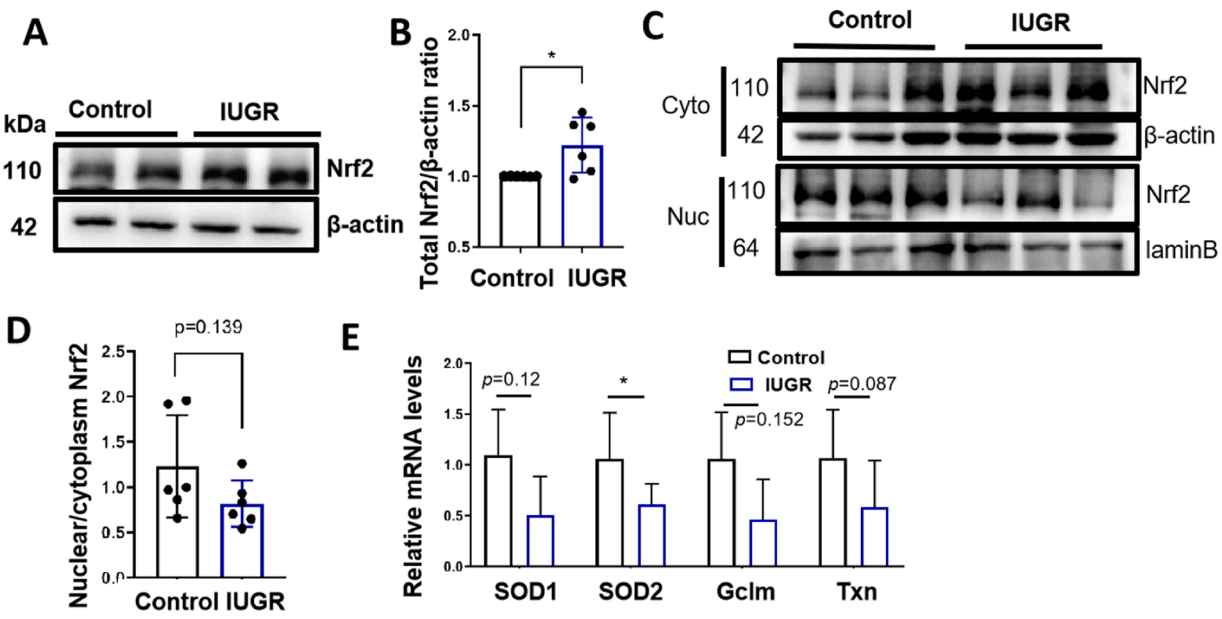

Fig. 3. Pulmonary Nrf2 nuclear translocation was blocked in lung tissue of IUGR offspring mice. (A-B) The protein expression of total Nrf2, β-actin was used as a loading control (n=6). (C-D) The protein expression of Nrf2 in cytoplasm and nucleus. LaminB was used as a nuclear loading control and β-actin was used as a cytoplasmic loading control. Nuclear/cytoplasm Nrf2=(Nuclear Nrf2/ LaminB) /(cytoplasm Nrf2/β-actin) (n=6). (E) mRNA expressions of oxidative stress related genes (control group, n=4; IUGR group, n=5). The data represent the mean±SD. Unpaired 2-sided t-test. Individual P-values are denoted above the comparison lines (*$P < 0.05$ vs control, **$P < 0.01$ vs control).

($P<0.0001$, WT IUGR VS Nrf2$^{-/-}$ IUGR) compared to WT mice (Fig. 5A and B). Additionally, Nrf2$^{-/-}$ offspring exhibited a significant reduction in body weight under hypoxic exposure, as shown in Fig. 5C and D ($P=0.0062$, WT IUGR VS Nrf2$^{-/-}$ IUGR, Fig. 5D). Importantly, Nrf2 knockout further aggravated pulmonary dysplasia characterized by alveolar simplification, thickened alveolar septum, and reduced number of alveoli (Fig. 5E). These findings indicate that Nrf2 deficiency exacerbates pulmonary dysplasia in IUGR offspring.

4. Discussion

The present study was designed to examine the roles and the mechanisms of Nrf2 on pulmonary complications in maternal hypoxia-induced IUGR offspring. Here, antenatal maternal hypoxia was used to mimic IUGR model, and we found that (1) antenatal maternal hypoxia inhibits Nrf2 nuclear translocation, leading to pyroptosis and resulting in pulmonary dysplasia in IUGR offspring; (2) Nrf2 inhibits GSDMD transcription and Nrf2 deficiency up-regulates the GSDMD expression and exacerbates pyroptosis in maternal hypoxia-induced IUGR offspring; (3) Nrf2 deficiency aggravated maternal hypoxia-induced pulmonary dysplasia in IUGR offspring. These results suggest that targeting Nrf2 may hold potential as a therapeutic approach for alleviating maternal hypoxia-induced pulmonary development retardation in IUGR offspring.

The NLRP3 and apoptosis-associated speck-like protein containing (ASC) collaborate to activate caspase-1, which cleaves GSDMD and releases the N-domain with pore-punching activity. The activating GSDMD-N forms pores in the cell membrane, leading to the release of IL-1β and IL-18 from the cell[11]. The NLRP3/caspase-1/GSDMD axis is a classical pathway that induces pyroptosis, which can occur in cases of sterile intra-amniotic inflammation and intra-amniotic infection in patients with spontaneous preterm labor and birth[37]. Activation of the NLRP3 inflammasome has been shown to be essential for the pathogenesis of bronchopulmonary dysplasia, a common complication of IUGR[5,38]. In this study, we observed upregulation of NLRP3, caspase-1, and GSDMD expression in lung tissues from IUGR offspring. Furthermore, we found significant upregulation of GSDMD-N at the cell membrane in IUGR lung tissues. Additionally, analysis using GEO database revealed high expression levels of GSDMD in IUGR placenta. These findings collectively suggest that antenatal maternal hypoxia triggers pyroptosis in IUGR offspring.

Nrf2, a key molecule that activates the expressions of downstream antioxidant stress genes[39], has been found to exhibit increased cytoplasmic expression in invasive extravillous trophoblasts associated with severe early onset IUGR and preeclampsia[40]. The activation of Nrf2 pathway through food supplements such as curcumin, docosahexaenoic acid, N-carbamylglutamate, and L-arginine has shown improvement in IUGR[29,41,42]. However, in a maternal hypoxia-induced IUGR mouse model, we observed an increase in total protein expression of Nrf2 but reduced nuclear translocation in lung tissues affected by IUGR. This indicates that Nrf2 fails to perform its transcription factor function. Furthermore, the deficiency of Nrf2 exacerbates IUGR and subsequent pulmonary dysplasia, emphasizing the crucial role of Nrf2 in improving pulmonary complications associated with IUGR.

Recent studies have demonstrated the pivotal role of Nrf2 in inhibiting NLRP3-mediated pyroptosis, which is implicated in sepsis[43], acute liver injury[44], and smoking-induced atherosclerosis[45]. Classical activators of Nrf2, such as sulforaphane[46] and dimethyl fumarate [47], have been reported to effectively suppress pyroptosis. Dimethyl fumarate has exhibited protective effects against lipopolysaccharide-induced shock, familial Mediterranean fever, and experimental autoimmune encephalitis by interacting with GSDMD [48]. However, the regulatory mechanism underlying the influence of Nrf2 on pyroptosis remains elusive. In this study, we discovered that Nrf2 represses the transcription and expression of GSDMD, and its knockout significantly exacerbates pyroptosis as evidenced by increased levels of caspase1, GSDMD, and IL-18. Overall, our findings provide novel evidence that deficiency in Nrf2 exacerbates pyroptosis in maternal hypoxia-induced IUGR offspring.

There are some limitations in this study. Firstly, although we found for the first time that the nuclear translocation of Nrf2 was impaired in maternal hypoxia-induced lung tissue, the specific molecular mechanism has not been studied. Secondly, effective measures to promote Nrf2 to enter the nucleus have not been explored. Thirdly, Nrf2 knockout

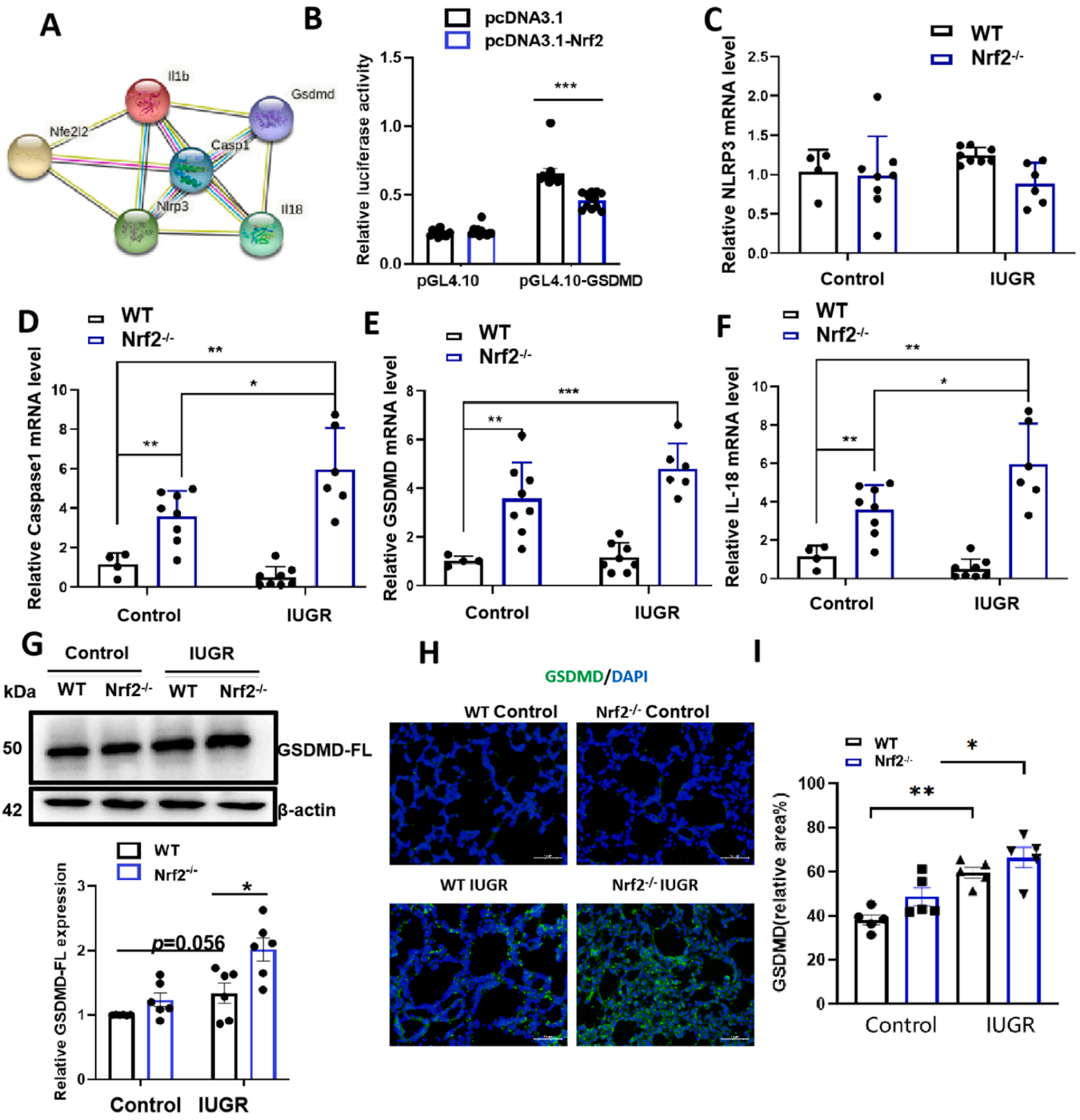

Fig. 4. Knockout of Nrf2 aggravated pyroptosis in the lung of maternal hypoxia-induced IUGR mice. (A) The protein-protein interaction (PPI) network of Nrf2, NLRP3, Caspase1, GSDMD, IL-18 and IL-1β (String). (B) The Nrf2 binding to the 3'-UTR of GSDMD was verified by the dual-luciferase reporter assay (n=8). (C-F) The mRNA levels of pyroptosis-related genes (WT control group, n=4; WT IUGR group, n=8; $Nrf2^{-/-}$ control group, n=8; $Nrf2^{-/-}$IUGR group, n=6). (G) The protein expression of GSDMD-FL was measured by western blotting (n=6). (H) Representative images of immunofluorescence staining of GSDMD (green). Nuclei were stained with DAPI (blue) (magnification, ×400). (I) Relative quantification of GSDMD fluorescence intensity (n=5). The data represent the mean ± SD, n=3–8 per group. One-way ANOVA. Individual P-values are denoted above the comparison lines (*$P < 0.05$; **$P < 0.01$ vs control; ***$P < 0.001$ vs control).

mice were used in this study, Nrf2 conditional knockout mice in alveolar epithelial cells or pulmonary vascular endothelial cells should be used in future studies. Finally, we analyzed the correlation between GSDMD and maternal hypoxia-induced IUGR using GEO database, multi-center clinical studies are needed to confirm the role of nrf2/GSDMD pathway in maternal hypoxia-induced IUGR.

In conclusion, our findings reveal that Nrf2 deficiency aggravated pyroptosis and pulmonary dysplasia in maternal hypoxia-induced fetal growth restriction. Nrf2 maybe a potential therapeutic target for hypoxia-induced pulmonary development retardation in IUGR offspring.

Ethics approval and consent to participate

All experiments were conducted in accordance with established guidelines and approved by the Animal Care and Use Committee of

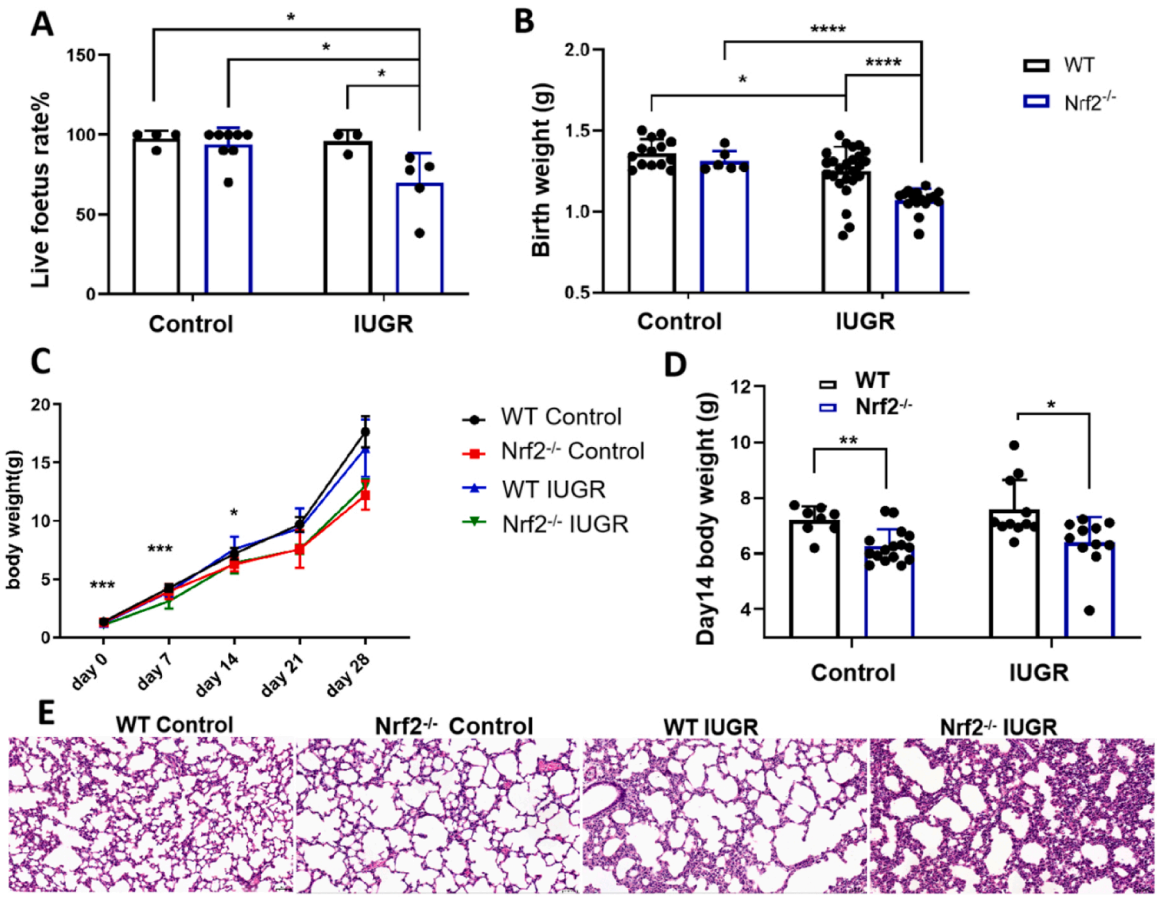

Fig. 5. Knockout of Nrf2 gene aggravated maternal hypoxia-induced IUGR and pulmonary dysplasia. (A) Live fetus rate of normoxic and hypoxic pups (WT control group, n=4; WT IUGR group, n=3; Nrf2$^{-/-}$ control group, n=8; Nrf2$^{-/-}$IUGR group, n=5). (B) Birth weight (WT control group, n=14; WT IUGR group, n=25; Nrf2$^{-/-}$ control group, n=6; Nrf2$^{-/-}$IUGR group, n=16). (C) Body weight. * indicates that there is a statistical difference between WT IUGR and Nrf2$^{-/-}$ IUGR. (D) Day 14 body weight(WT control group, n=8; WT IUGR group, n=11; Nrf2$^{-/-}$ control group, n=16; Nrf2$^{-/-}$IUGR group, n=11). (E) Representative H&E stained lung sections (magnification, ×200). The data represent the mean ± SD. One-way ANOVA. Individual P-values are denoted above the comparison lines (*$P < 0.05$; **$P < 0.01$; ***$P < 0.001$).

Jiangnan University (JN.No20201130c0420720[325]). All the authors consented to participate in this study.

Fundings

This study was supported by National Natural Science Foundation of China (81901522, 82171704, 82100018). Natural Science Foundation of Jiangsu Province (BK20200602). Fundamental Research Funds for the Central Universities (JUSRP121062). Zhejiang Medicine and Health Science and Technology Project (2023KY1217, 2023AD31118, 2023AD30131).

Declaration of Competing Interest

The authors declare that they have no known competing financial interests or personal relationships that could have appeared to influence the work reported in this paper.

Data Availability

The datasets used and/or analyzed during the current study are available from the corresponding author on reasonable request.

Appendix A. Supporting information

Supplementary data associated with this article can be found in the online version at doi:10.1016/j.reprotox.2024.108671.

References

[1] R. Goyal, A. Leitzke, D. Goyal, C.P. Gheorghe, L.D. Longo, Antenatal maternal hypoxic stress: adaptations in fetal lung Renin-Angiotensin system, Reprod. Sci. Thousand Oaks Calif. 18 (2011) 180–189, https://doi.org/10.1177/1933719110385134.

[2] Fetal Growth Restriction: ACOG Practice Bulletin, Number 227, Obstet. Gynecol. 137 (2021) e16-e28. https://doi.org/10.1097/AOG.0000000000042512021.

[3] L.A. Joss-Moore, Y. Wang, X. Yu, M.S. Campbell, C.W. Callaway, R.A. McKnight, A. Wint, M.J. Dahl, R.O. Dull, K.H. Albertine, R.H. Lane, IUGR decreases elastin mRNA expression in the developing rat lung and alters elastin content and lung compliance in the mature rat lung, Physiol. Genom. 43 (2011) 499–505, https://doi.org/10.1152/physiolgenomics.00183.2010.

[4] E. Ronkainen, T. Dunder, T. Kaukola, R. Marttila, M. Hallman, Intrauterine growth restriction predicts lower lung function at school age in children born very preterm, Arch. Dis. Child. Fetal Neonatal Ed. 101 (2016) F412–F417, https://doi.org/10.1136/archdischild-2015-308922.

[5] K. Pike, J. Jane Pillow, J.S. Lucas, Long term respiratory consequences of intrauterine growth restriction, Semin. Fetal Neonatal Med. 17 (2012) 92–98, https://doi.org/10.1016/j.siny.2012.01.003.

[6] M. Arigliani, C. Stocco, E. Valentini, C. De Pieri, L. Castriotta, M.E. Ferrari, C. Canciani, L. Driul, M. Orsaria, L. Cattarossi, P. Cogo, Lung function between 8 and 15 years of age in very preterm infants with fetal growth restriction, Pediatr. Res. 90 (2021) 657–663, https://doi.org/10.1038/s41390-020-01299-0.

[7] G.S. Maritz, M.L. Cock, S. Louey, K. Suzuki, R. Harding, Fetal growth restriction has long-term effects on postnatal lung structure in sheep, Pediatr. Res. 55 (2004) 287–295, https://doi.org/10.1203/01.PDR.0000106314.99930.65.

[8] S. Orgeig, T.A. Crittenden, C. Marchant, I.C. McMillen, J.L. Morrison, Intrauterine growth restriction delays surfactant protein maturation in the sheep fetus, Am. J. Physiol. Lung Cell. Mol. Physiol. 298 (2010) L575–L583, https://doi.org/10.1152/ajplung.00226.2009.

[9] X.F. Xu, Y. Lv, W.Z. Gu, L.L. Tang, J.K. Wei, L.Y. Zhang, L.Z. Du, Epigenetics of hypoxic pulmonary arterial hypertension following intrauterine growth retardation rat: epigenetics in PAH following IUGR, Respir. Res. 14 (2013) 20, https://doi.org/10.1186/1465-9921-14-20.

[10] Jack R.T. Darby, Tamara J. Varcoe, Sandra Orgeig, Janna L. Morrison, Cardiorespiratory consequences of intrauterine growth restriction: influence of timing, severity and duration of hypoxaemia, Theriogenology 150 (2020) 84–95.

[11] S. Bedoui, M.J. Herold, A. Strasser, Emerging connectivity of programmed cell death pathways and its physiological implications, Nat. Rev. Mol. Cell Biol. 21 (2020) 678–695, https://doi.org/10.1038/s41580-020-0270-8.

[12] J. Shi, W. Gao, F. Shao, Pyroptosis: gasdermin-mediated programmed necrotic cell death, Trends Biochem. Sci. 42 (2017) 245–254, https://doi.org/10.1016/j.tibs.2016.10.004.

[13] Y. Lou, J. Miao, F. Li, J. Ding, L. Wang, Maternal smoking during pregnancy aggravated muscle phenotype in FHL1-/y offspring mice similar to congenital clubfoot through P2RX7-mediated pyroptosis, Toxicol. Lett. 345 (2021) 54–60, https://doi.org/10.1016/j.toxlet.2021.04.014.

[14] T. Zhang, L. Sun, T. Wang, C. Liu, H. Zhang, C. Zhang, L. Yu, Gestational exposure to PM2.5 leads to cognitive dysfunction in mice offspring via promoting HMGB1-NLRP3 axis mediated hippocampal inflammation, Ecotoxicol. Environ. Saf. 223 (2021) 112617, https://doi.org/10.1016/j.ecoenv.2021.112617.

[15] J. Wei, W. Zheng, C. Teng, X. An, L. Li, P. Zhong, C. Peng, S. Zhuge, J. Akoto Ampadu, C. Yu, X. Cai, Exogenous NADPH could mitigate pyroptosis-induced brain injury in fetal mice exposed to gestational intermittent hypoxia, Int. Immunopharmacol. 135 (2024) 112311, https://doi.org/10.1016/j.intimp.2024.112311.

[16] Y.Q. Su, Y. Lin, S.J. Huang, Y.T. Lin, J. Ran, F.F. Yan, X.L. Liu, L.C. Hong, M. Huang, H.Z. Su, X.D. Zhang, J.H. You, Y.M. Su, Pyroptosis is involved in maternal nicotine exposure-induced metabolic associated fatty liver disease progression in offspring mice, Mol. Reprod. Dev. (2023), https://doi.org/10.1002/mrd.23719.

[17] Y. Shan, P. Liu, Y. Zhou, X. Ding, H. Liu, J. Yang, Prenatal sevoflurane exposure impairs the learning and memory of rat offspring via HMGB1-induced NLRP3/ASC inflammasome activation, ACS Chem. Neurosci. 14 (2023) 699–708, https://doi.org/10.1021/acschemneuro.2c00620.

[18] H. Zhang, H. Lu, L. Yu, J. Yuan, S. Qin, C. Li, R.-S. Ge, H. Chen, L. Ye, Effects of gestational exposure to perfluorooctane sulfonate on the lung development of offspring rats, Environ. Pollut. Barking Essex 1987 272 (2021) 115535, https://doi.org/10.1016/j.envpol.2020.115535.

[19] Cong Li, Huishan Zhang, Jiali Mo, Jingye Zuo, Leping Ye, Caspase-3/GSDME dependent pyroptosis contributes to offspring lung injury induced by gestational PFOS exposure via PERK/ATF4 signaling, Arch. Toxicol. 98 (1) (2024 Jan) 207–221.

[20] J. Sun, Y. Li, Pyroptosis and respiratory diseases: a review of current knowledge, Front. Immunol. 13 (2022) 920464, https://doi.org/10.3389/fimmu.2022.920464.

[21] J. Wu, Y. Lan, J. Wu, K. Zhu, Sepsis-induced acute lung injury is alleviated by small molecules from dietary plants via pyroptosis modulation, J. Agric. Food Chem. 71 (2023) 12153–12166, https://doi.org/10.1021/acs.jafc.2c08926.

[22] B.B. Kobal, İ. Kale, A.M. Pektaş, A. Ozel, M. Muhcu, Maternal serum gasdermin D concentrations in pregnancies complicated by isolated intrauterine growth restriction, Z. Geburtshilfe Neonatol. 227 (2023) 197–203, https://doi.org/10.1055/a-1967-2274.

[23] K. Tian, Y. Yang, K. Zhou, N. Deng, Z. Tian, Z. Wu, X. Liu, F. Zhang, Z. Jiang, The role of ROS-induced pyroptosis in CVD, Front. Cardiovasc. Med. 10 (2023) 1116509, https://doi.org/10.3389/fcvm.2023.1116509.

[24] Z. Yin, B. Wan, G. Gong, J. Yin, ROS: Executioner of regulating cell death in spinal cord injury, Front. Immunol. 15 (2024) 1330678, https://doi.org/10.3389/fimmu.2024.1330678.

[25] N.K. Grilc, M. Sova, J. Kristl, Drug delivery strategies for curcumin and other natural Nrf2 modulators of oxidative stress-related diseases, Pharmaceutics 13 (2021) 2137, https://doi.org/10.3390/pharmaceutics13122137.

[26] Klaudia Jomova, Renata Raptova, Suliman Y. Alomar, Saleh H. Alwasel, Eugenie Nepovimova, Kamil Kuca, Marian Valko, Reactive oxygen species, toxicity, oxidative stress, and antioxidants: chronic diseases and aging, Arch. Toxicol. 97 (10) (2023 Oct) 2499–2574.

[27] Q. Liu, Y. Gao, X. Ci, Role of Nrf2 and its activators in respiratory diseases, Oxid. Med. Cell. Longev. 2019 (2019) 7090534, https://doi.org/10.1155/2019/7090534.

[28] N. Kweider, B. Huppertz, W. Rath, J. Lambertz, R. Caspers, M. ElMoursi, U. Pecks, M. Kadyrov, A. Fragoulis, T. Pufe, C.J. Wruck, The effects of Nrf2 deletion on placental morphology and exchange capacity in the mouse, J. Matern. Fetal Neonatal Med. J. Eur. Assoc. Perinat. Med. Fed. Asia Ocean. Perinat. Soc. Int. Soc. Perinat. Obstet. 30 (2017) 2068–2073, https://doi.org/10.1080/14767058.2016.1236251.

[29] Y. Niu, J. He, H. Ahmad, M. Shen, Y. Zhao, Z. Gan, L. Zhang, X. Zhong, C. Wang, T. Wang, Dietary curcumin supplementation increases antioxidant capacity, upregulates Nrf2 and Hmox1 levels in the liver of piglet model with intrauterine growth retardation, Nutrients 11 (2019) 2978, https://doi.org/10.3390/nu11122978.

[30] L. Zhang, J. Zhang, E. Yan, J. He, X. Zhong, L. Zhang, C. Wang, T. Wang, Dietary supplemented curcumin improves meat quality and antioxidant status of intrauterine growth retardation growing pigs via Nrf2 signal pathway, Anim. Open Access J. MDPI 10 (2020) 539, https://doi.org/10.3390/ani10030539.

[31] M. Wang, F. Zhang, X. Ning, C. Wu, Y. Zhou, Z. Gou, Y. Fan, R. Duan, Z. Li, C. Shao, L. Lu, Regulating NLRP3 inflammasome-induced pyroptosis via Nrf2: TBHQ limits hyperoxia-induced lung injury in a mouse model of bronchopulmonary dysplasia, Inflammation 46 (2023) 2386–2401, https:// doi.org/ 10.1007/ s10753-023-01885-4.

[32] K.C.W. Wang, A.N. Larcombe, L.J. Berry, J.S. Morton, S.T. Davidge, A.L. James, P. B. Noble, Foetal growth restriction in mice modifies postnatal airway responsiveness in an age and sex-dependent manner, Clin. Sci. Lond. Engl. 1979 132 (2018) 273–284, https://doi.org/10.1042/CS20171554.

[33] D. Chen, Y.-Y. Wang, S.-P. Li, H.-M. Zhao, F.-J. Jiang, Y.-X. Wu, Y. Tong, Q.-F. Pang, Maternal propionate supplementation ameliorates glucose and lipid metabolic disturbance in hypoxia-induced fetal growth restriction, Food Funct. 13 (2022) 10724–10736, https://doi.org/10.1039/d2fo01481e.

[34] Dan Chen, et al., Sodium propionate enhances Nrf2-mediated protective defense against oxidative stress and inflammation in lipopolysaccharide-induced neonatal mice, J. Inflamm. Res 14 (2021 Mar 10) 803–816.

[35] Damian Szklarczyk, Andrea Franceschini, Stefan Wyder, Kristoffer Forslund, Davide Heller, Jaime Huerta-Cepas, Milan Simonovic, Alexander Roth, Alberto Santos, Kalliopi P. Tsafou, Michael Kuhn, Peer Bork, Lars J. Jensen, Christian von Mering, STRING v10: protein-protein interaction networks, integrated over the tree of life. Nucleic Acids Res 43 (Database issue) (2015 Jan) D447–D452.

[36] J.B. Wu, Y.L. Tang, X.H. Liang, Targeting VEGF pathway to normalize the vasculature: an emerging insight in cancer therapy, OncoTargets Ther. 11 (2018) 6901–6909, https://doi.org/10.2147/OTT.S172042.

[37] Nardhy Gomez-Lopez, Roberto Romero, Adi L. Tarca, Derek Miller, Bogdan Panaitescu, George Schwenkel, Dereje W. Gudicha, Sonia S. Hassan, Percy Pacora, Eunjung Jung, Chaur-Dong Hsu, Gasdermin D: evidence of pyroptosis in spontaneous preterm labor with sterile intra-amniotic inflammation or intra-amniotic infection, Am. J. Reprod. Immunol. 82 (6) (2019 Dec) e13184.

[38] S. Chen, Q. Wu, D. Zhong, C. Li, L. Du, Caffeine prevents hyperoxia-induced lung injury in neonatal mice through NLRP3 inflammasome and NF-κB pathway, Respir. Res. 21 (2020) 140, https://doi.org/10.1186/s12931-020-01403-2.

[39] T. Suzuki, H. Motohashi, M. Yamamoto, Toward clinical application of the Keap1-Nrf2 pathway, Trends Pharmacol. Sci. 34 (2013) 340–346, https://doi.org/10.1016/j.tips.2013.04.005.

[40] N. Kweider, B. Huppertz, C.J. Wruck, R. Beckmann, W. Rath, T. Pufe, M. Kadyrov, A role for Nrf2 in redox signalling of the invasive extravillous trophoblast in severe early onset IUGR associated with preeclampsia, PloS One 7 (2012) e47055, https://doi.org/10.1371/journal.pone.0047055.

[41] W. Jiang, L. Wan, P. Chen, W. Lu, Docosahexaenoic acid activates the Nrf2 signaling pathway to alleviate impairment of spleen cellular immunity in intrauterine growth restricted rat pups, Saudi J. Biol. Sci. 28 (2021) 4987–4993, https://doi.org/10.1016/j.sjbs.2021.05.058.

[42] H. Zhang, H. Sun, A. Peng, S. Guo, M. Wang, J.J. Loor, H. Wang, N-carbamylglutamate and l-arginine promote intestinal function in suckling lambs with intrauterine growth restriction by regulating antioxidant capacity via a nitric oxide-dependent pathway, Food Funct. 10 (2019) 6374–6384, https://doi.org/10.1039/c9fo01752f.

[43] Y. Teng, N. Li, Y. Wang, S. Sun, J. Hou, Y. Chen, H. Pan, NRF2 inhibits cardiomyocyte pyroptosis via regulating CTRP1 in sepsis-induced myocardial injury, Shock Augusta Ga 57 (2022) 590–599, https://doi.org/10.1097/SHK.0000000000001901.

[44] W. Yang, K. Tao, P. Zhang, X. Chen, X. Sun, R. Li, Maresin 1 protects against lipopolysaccharide/d-galactosamine-induced acute liver injury by inhibiting macrophage pyroptosis and inflammatory response, Biochem. Pharmacol. 195 (2022) 114863, https://doi.org/10.1016/j.bcp.2021.114863.

[45] Zhewei Zhao, Xuebin Wang, Rui Zhang, 1, Baitao Ma, Shuai Niu, Xiao Di, Leng Ni, Changwei Liu, Melatonin attenuates smoking-induced atherosclerosis by activating the Nrf2 pathway via NLRP3 inflammasomes in endothelial cells, Aging (Albany NY) 13 (8) (2021 Apr 4) 11363–11380.

[46] K.U. Tufekci, I. Ercan, K.B. Isci, M. Olcum, B. Tastan, C.P. Gonul, K. Genc, S. Genc, Sulforaphane inhibits NLRP3 inflammasome activation in microglia through Nrf2-mediated miRNA alteration, Immunol. Lett. 233 (2021) 20–30, https://doi.org/10.1016/j.imlet.2021.03.004.

[47] B. Tastan, B.I. Arioz, K.U. Tufekci, E. Tarakcioglu, C.P. Gonul, K. Genc, S. Genc, Dimethyl Fumarate alleviates NLRP3 inflammasome activation in microglia and sickness behavior in LPS-challenged mice, Front. Immunol. 12 (2021) 737065, https://doi.org/10.3389/fimmu.2021.737065.

[48] F. Humphries, L. Shmuel-Galia, N. Ketelut-Carneiro, S. Li, B. Wang, V.V. Nemmara, R. Wilson, Z. Jiang, F. Khalighinejad, K. Muneeruddin, S.A. Shaffer, R. Dutta, C. Ionete, S. Pesiridis, S. Yang, P.R. Thompson, K.A. Fitzgerald, Succination inactivates gasdermin D and blocks pyroptosis, Science 369 (2020) 1633–1637, https://doi.org/10.1126/science.abb9818.